J. Fluid Mech. (1986), *vol.* 173, *pp.* 643–666
Printed in Great Britain

Acoustic emissions by vortex motions

By T. KAMBE
Department of Physics, University of Tokyo, Hongo, Bunkyo-ku, Tokyo 113, Japan

(Received 17 April 1986)

Fundamental aspects of the acoustic emission by vortex motions are considered by summarizing our recent work. Three typical cases are presented as illustrative examples: (i) head-on collision of two vortex rings, (ii) a vortex ring moving near a circular cylinder, and (iii) a vortex ring moving near a sharp edge of a semi-infinite plate. The theory of aerodynamic sound for low-Mach-number motion of an inviscid fluid predicts that the amplitude of the acoustic pressure in the far field is proportional to U^4, U^3 and $U^{2.5}$ for (i)–(iii) respectively, where U is the translation velocity of a single vortex ring. Therefore the vortex–edge interaction generates the most powerful sound among the three cases at low Mach numbers. Our observations have confirmed these scaling laws. In addition to the scaling properties, we show the wave profiles of the emission as well as the directionality pattern. The head-on collision radiates waves of quadrupole directionality, whereas waves of dipole property are originated by the vortex–cylinder interaction. The third, vortex–edge, interaction generates waves of a cardioid directionality pattern. The wave profiles of all three cases are related to the time derivatives of the volume flux (through the vortex ring) of an imaginary potential flow which is characteristic of each configuration, although the orders of the time derivatives are different for each case. The observed profiles are surprisingly well fitted to the curves predicted by the theory, except the final period of the first case, in which viscosity is assumed to play an important role. The observed wave profiles are shown in a perspective diagram.

1. Introduction

We consider here the acoustic emission by vortex motions in the presence or absence of a solid body at rest, based on the fundamental equations of motion at low Mach numbers. The physical idea is as follows. Suppose that there exists an unsteady fluid motion with localized vorticity $\boldsymbol{\omega}$, which induces a nearly incompressible velocity field $\boldsymbol{v}$. Pressure fluctuations are originated at large distances or on the body surfaces by the unsteady flow. These drive acoustic waves, forming an extensive sound field. The problem of sound emission in general depends on four length parameters: the vortex size l, a dimension l_* of the region containing vorticity, the body size L and the wavelength λ of the sound. Here the ratio l/l_* is assumed to be of order unity. If u is a representative velocity of the flow, then the timescale of the vortex motion is $\tau = l/u$. The length of the wave being generated will be $\lambda = c\tau = l/M$, where $M = u/c$, and c is the sound speed. It is assumed that the Mach number M is much less than unity:

$$M = \frac{u}{c} \ll 1. \tag{1.1}$$

This leads to separation of two regions owing to the relation $\lambda \gg l$. The rotational flow scaled on l can be visualized as an inner region, surrounded by an outer wavefield

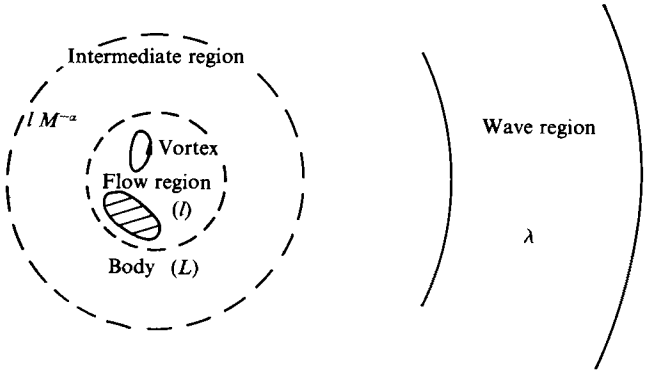

FIGURE 1. Schematic diagram of the inner flow region and the outer wave region ($l/\lambda = M \ll 1$, $0 < \alpha < 1$).

scaled on λ (figure 1). This situation admits analyses based on the method of matched asymptotic expansions, which were developed independently by Crow (1970), Obermeier (1967), Müller & Obermeier (1967) and Lauvstad (1968), and subsequently studied by Möhring, Müller & Obermeier (1969), Crighton (1972), Obermeier (1976, 1979, 1980) and Kambe & Minota (1981). In particular, Crow showed that the outer acoustic field is equivalent to that generated by the distribution of quadrupole of strength $\rho_0 v_i v_j$, which was first proposed by Lighthill (1952) in a rather broad sense, where ρ_0 is the unperturbed uniform density. Further it was shown by Howe (1975*b*) that the source of the form div $(\boldsymbol{\omega} \times \boldsymbol{v})$, proposed first by Powell (1964), can be related to Lighthill's source $\partial^2(\rho_0 v_i v_j)/\partial x_i \partial x_j$.

Lighthill's pioneering work (1952) was based on an inhomogeneous wave equation with source terms, without recourse to the method of matched asymptotic expansions. Most subsequent work followed this approach, e.g. Curle (1955), Ffowcs Williams (1969), Howe (1975*b*) etc. In particular, starting from Lighthill's theory Möhring (1978) found an expression for the acoustic pressure solely in terms of the vorticity without involving the velocity.

The present paper is concerned with three typical problems, namely the sound emissions by vortex motion (i) in the absence of a solid body, (ii) in the presence of a solid body of size L ($\approx l$), and (iii) in the presence of an edged body of semi-infinite extent. As illustrative examples, we consider the motion of vortex rings and present observations from corresponding experiments.

Within the framework of the method of matched asymptotic expansions (except for case (iii)), we present a reformulation of the theory of vortex sound, based on the ideas of Obermeier (1976, 1979, 1980), Möhring (1978), Kambe & Minota (1981), and apply it to the present problems concerned with vortex rings. In their formulations, Möhring and Obermeier introduced a vector Green function. It is shown here that an equivalent formulation can be done without using a special notion of the vector Green function, i.e. such a vector function is naturally introduced in the problem as a vector potential of a certain velocity field. In particular, it is found that temporal pressure profiles of the acoustic emission by vortices are related to the time derivatives of the volume flux (through the vortex loops) of an imaginary potential flow, which is characteristic of each configuration. This will be a new description of the acoustic pressure; however the main body of this article is a review of our recent work. It is remarkable that the main features of the theoretical predictions are

reproduced in the laboratory experiments for the three cases that used vortex rings. The experiments are briefly described here; and the details may be found in the referenced papers.

In §2 governing equations of the inner and outer region are presented. The method of matched asymptotic expansions is developed in §3 in the context of the present problem of vortex sound. Acoustic emission by vortices in free space is considered in §4, while §5 is concerned with the sound emission from the vortex–body interaction. The edge effect on the wavefield is considered in §6 for a semi-infinite plate.

2. Flow field and wavefield

We consider the flow of an inviscid fluid, which is governed by

$$\frac{\partial \rho}{\partial t}+\frac{\partial}{\partial x_i}\rho v_i = 0, \tag{2.1}$$

$$\frac{\partial}{\partial t}\rho v_i+\frac{\partial}{\partial x_j}\rho v_i v_j = -\frac{\partial p}{\partial x_i}, \tag{2.2}$$

$$\mathrm{d}p = c^2\,\mathrm{d}\rho, \tag{2.3}$$

where ρ is density, p pressure and $c = (\partial p/\partial\rho)_s^{\frac{1}{2}}$ the sound speed (the entropy s is preserved in the inviscid fluid flow), and a summation convention is used. On eliminating the ρv_i terms in the above equations and replacing ρ_{tt} by p_{tt}/c^2 (where $p_{tt} = \partial^2 p/\partial t^2$, etc), we obtain the inhomogeneous wave equation for p:

$$\frac{1}{c^2}\frac{\partial^2 p}{\partial t^2}-\nabla^2 p = \frac{\partial^2}{\partial x_i\,\partial x_j}(\rho v_i v_j) \tag{2.4}$$

(Lighthill 1952). This is the basic equation for the acoustic emission in the present context. The fluid at rest is characterized by a uniform density ρ_0, pressure p_0 and sound speed c. On the assumption of a low Mach number (1.1), the density ρ on the right-hand side of (2.4) is replaced by the uniform value ρ_0, neglecting the terms of order M^2. Thus we have

$$\frac{1}{c^2}\frac{\partial^2}{\partial t^2}p-\nabla^2 p = \rho_0\frac{\partial^2}{\partial x_i\,\partial x_j}v_i v_j. \tag{2.5}$$

In the inner region scaled on l, we define the following inner variables:

$$x_i' = \frac{x_i}{l}\quad\left(x' = \frac{x}{l}\right),\quad t' = \frac{t}{\tau},\quad p' = \frac{p-p_0}{\rho_0 u^2},\quad v_i' = \frac{v_i}{u},\quad \nabla' = l\nabla, \tag{2.6}$$

using primed notation for the other inner variables. Equation (2.5) is rewritten as

$$\nabla'^2 p' = -\frac{\partial^2}{\partial x_i'\,\partial x_j'}v_i' v_j' + O(M^2). \tag{2.7}$$

This is equivalent to taking $c = \infty$. It should be noted that the same equation without the $O(M^2)$ term can be derived as the governing equation for an incompressible fluid.

For later use, let us consider a solenoidal velocity field $\boldsymbol{v}$ induced by a vorticity distribution $\boldsymbol{\omega}$, which is given at an initial instant in a bounded domain D_0 of linear dimension $O(l)$ and stays in a bounded domain D at subsequent times. The vorticity

$\boldsymbol{\omega}$ develops subsequently according to Euler's equation of motion. Introducing a vector potential $\boldsymbol{A}$, the velocity $\boldsymbol{v}$ is expressed as

$$\boldsymbol{v}(\boldsymbol{x},t) = \operatorname{rot}\boldsymbol{A}, \quad \boldsymbol{A}(\boldsymbol{x},t) = \frac{1}{4\pi}\int \frac{\boldsymbol{\omega}(\boldsymbol{y},t)}{|\boldsymbol{x}-\boldsymbol{y}|}\,\mathrm{d}^3\boldsymbol{y}. \tag{2.8}$$

This velocity field is solenoidal, i.e. $\operatorname{div}\boldsymbol{v} = 0$ (evidently $\operatorname{rot}\boldsymbol{v} = \boldsymbol{\omega}$). Using the vector $\boldsymbol{y}$ as a position vector in the domain D, an asymptotic expression for $\boldsymbol{A}(\boldsymbol{x},t)$ at large distances from D is obtained using the expansion

$$|\boldsymbol{x}-\boldsymbol{y}|^{-1} = \frac{1}{x} - y_i\frac{\partial}{\partial x_i}\frac{1}{x} + \tfrac{1}{2}y_i y_j \frac{\partial^2}{\partial x_i \partial x_j}\frac{1}{x} + \dots, \tag{2.9}$$

where $x = |\boldsymbol{x}|$ is assumed much larger than $y = |\boldsymbol{y}|$. Outside D, the velocity is irrotational and is represented by the form $\boldsymbol{v} = \operatorname{grad}\Phi$. The velocity potential Φ associated with the vorticity distribution $\boldsymbol{\omega}(\boldsymbol{x},t)$ is given by the series expansion at large values of x:

$$\Phi = \frac{1}{4\pi}P_i\frac{\partial}{\partial x_i}\frac{1}{x} - Q_{ij}\frac{\partial^2}{\partial x_i \partial x_j}\frac{1}{x} + O(x^{-4}), \tag{2.10}$$

where

$$P_i = \frac{1}{2}\int (\boldsymbol{y}\times\boldsymbol{\omega})_i\,\mathrm{d}^3\boldsymbol{y}, \quad Q_{ij} = \frac{1}{12\pi}\int y_i(\boldsymbol{y}\times\boldsymbol{\omega})_j\,\mathrm{d}^3\boldsymbol{y}. \tag{2.11}$$

The term corresponding to the first term of (2.9) vanishes owing to the property $\int \omega_i\,\mathrm{d}^3\boldsymbol{y} = 0$. The vector P_i is the flow impulse and the tensor Q_{ij}, having the property $Q_{ii} = 0$, is a second moment of the vorticity distribution, which will in §4 be related to the wave pressure generated by the vortex motion. In general they depend on the time t. In the absence of external forces and bodies, the impulse P_i is conserved. It will be shown that the excitation of an acoustic wave by an incompressible rotational flow (2.8) is closely related to the time dependence of the coefficients of the multipole expansion (2.10). It is obvious from (2.10) that the magnitude of $v_i = \partial\Phi/\partial x_i$ is $O(x^{-3})$ as $x\to\infty$.

Next, consider the system with a larger lengthscale. Using the scaling length λ, we obtain an estimate of magnitude

$$O\left(\frac{1}{c^2}p_{tt}\right)\Big/O(\nabla^2 p) = \frac{\lambda^2}{c^2\tau^2},$$

which is of order unity. Hence the two terms on the left-hand side of (2.5) are comparable in magnitude. In general, the pressure p associated with a compressible motion (therefore p_{tt}/c^2 also) decays as x^{-1}, whereas the velocity v_i on the right-hand side decays like $O(x^{-3})$ for the solenoidal component. The compressible velocity component (which is given by $p/\rho_0 c$ in the linear theory of sound) decays as $uM^{1+\beta}l/x$, where $\beta > 0$ will be shown later for the present cases. Introducing the outer variables defined by

$$\hat{x}_i = \frac{x_i}{\lambda} = x_i' M \quad \left(\hat{x} = \frac{x}{\lambda}\right), \quad \hat{t} = t' = \frac{t}{\tau}, \quad M = \frac{l}{\lambda},$$

$$\hat{p} = \frac{p-p_0}{\rho_0 u^2}, \quad \hat{v}_i = \frac{v_i}{u}, \quad \hat{\nabla} = \lambda\nabla,$$

we find that (2.5) is approximated by

$$\frac{\partial^2}{\partial \hat{t}^2}\hat{p} - \hat{\nabla}^2\hat{p} = 0 \tag{2.12}$$

Neglecting $O(M^{4+2\beta})$ terms relative to those retained. This equation is the wave equation, suggesting that there exists a region of wave propagation at large distances (Crow 1970).

3. Expressions of pressure

3.1. *Inner flow region*

The governing equations for the inner region are

$$\operatorname{div} \boldsymbol{v} = 0, \quad \frac{\partial}{\partial t}\boldsymbol{v} + (\boldsymbol{v}\cdot\boldsymbol{\nabla})\,\boldsymbol{v} = -\frac{1}{\rho_0}\boldsymbol{\nabla} p, \tag{3.1a,b}$$

in dimensional terms. Introducing the notation $\boldsymbol{L} = (\boldsymbol{v}\cdot\boldsymbol{\nabla})\,\boldsymbol{v}$, we have

$$\boldsymbol{L} = (\boldsymbol{v}\cdot\boldsymbol{\nabla})\,\boldsymbol{v} = \boldsymbol{\omega}\times\boldsymbol{v} + \operatorname{grad}\tfrac{1}{2}v^2. \tag{3.2}$$

Taking the rotation of (3.1*b*) yields the governing equation for $\boldsymbol{\omega}$:

$$\frac{\partial}{\partial t}\boldsymbol{\omega} + \boldsymbol{\nabla}\times(\boldsymbol{\omega}\times\boldsymbol{v}) = 0. \tag{3.3}$$

The pressure is determined by (2.7), which is rewritten as

$$\nabla^2 p = -\rho_0\,\boldsymbol{\nabla}\cdot\boldsymbol{L}, \tag{3.4}$$

since $\partial(v_i v_j)/\partial x_j = L_i$ by the solenoidal condition (3.1*a*). This is a Poisson-type equation for p. Introducing the Green function $G(\boldsymbol{x},\boldsymbol{y})$ satisfying $\nabla^2 G = -\delta(\boldsymbol{x}-\boldsymbol{y})$, we readily obtain the integral representation

$$p_{\mathrm{I}}(\boldsymbol{x},t) \equiv p - p_0 = \rho_0 \int G(\boldsymbol{x},\boldsymbol{y})\,\boldsymbol{\nabla}\cdot\boldsymbol{L}(\boldsymbol{y},t)\,\mathrm{d}^3\boldsymbol{y}, \tag{3.5}$$

where p_{I} denotes the deviation of pressure in the inner region from the uniform value p_0.

In the presence of a solid body, boundary conditions are imposed on the body surface S:

$$\boldsymbol{n}\cdot\boldsymbol{v} = 0 \quad \text{on } S, \tag{3.6}$$

$$\boldsymbol{n}\cdot\boldsymbol{\nabla}_y G = 0 \quad \text{for } \boldsymbol{y} \text{ on } S, \tag{3.7}$$

where $\boldsymbol{n}$ is a unit normal to S, where $\boldsymbol{\nabla}_y$ is the grad operator with respect to the vector $\boldsymbol{y}$. In this case an additional term of the surface integral (with y denoting integration variable)

$$\int_S G(\boldsymbol{n}\cdot\boldsymbol{\nabla}_y)\,p\,\mathrm{d}S \tag{3.8}$$

is to be added on the right-hand side of (3.5) by the Green theorem. Performing partial integration to the volume integral of (3.5) and using (3.1*b*) and (3.2) which give $\boldsymbol{n}\cdot(\rho_0\boldsymbol{L}+\boldsymbol{\nabla}p) = -\rho_0\,\partial(\boldsymbol{n}\cdot\boldsymbol{v})/\partial t = 0$ (on S), one finds that the surface integrals drop out, and obtains the pressure represented only by the volume integral:

$$p_{\mathrm{I}} = -\rho_0 \int \boldsymbol{L}(\boldsymbol{y},t)\cdot\boldsymbol{\nabla}_y G\,\mathrm{d}^3\boldsymbol{y}, \tag{3.9}$$

It is remarkable that this integral representation is valid whether a solid body is present or not.

3.2. *Outer wave region*

This region is described by the wave equation. A general representation of the solution is given in the form of a multipole expansion: namely, with an arbitrary function

$a(\hat{t})$ and $\hat{x} = |\hat{\boldsymbol{x}}|$, a function of the form $\hat{x}^{-1}a(\hat{t}-\hat{x}/c)$ is a solution of (2.12). Its derivative, obtained by differentiating arbitrary times with respect to the space coordinates $\hat{x}_i$, is also a solution. Thus the pressure ($p_{\mathrm{O}} = p - p_0$) of the acoustic wave in the outer region is represented in the form of multipole expansion:

$$p_{\mathrm{O}}(\hat{x},\hat{t}) = \frac{A_0(\hat{t}-\hat{x})}{\hat{x}} + \frac{\partial}{\partial \hat{x}_i}\frac{A_i(\hat{t}-\hat{x})}{\hat{x}} + \frac{\partial^2}{\partial \hat{x}_i\,\partial \hat{x}_j}\frac{A_{ij}(\hat{t}-\hat{x})}{\hat{x}} + \dots, \tag{3.10}$$

where $\hat{t}-\hat{x} = (t-x/c)/\tau$ is the retarded time in the outer variables. The functions $A_0(\hat{t}), A_i(\hat{t}), A_{ij}(\hat{t}), \dots$, having the dimension of pressure, are unknowns to be determined by matching to the inner solution p_{I}. In other words, this pressure formula represents the emission of acoustic waves by vortex motion if the functions $A_0, A_i, A_{ij}, \dots$ are determined in terms of the vortex motion.

3.3. *Matching procedure*

The matching of the two expressions $p_{\mathrm{I}}(\boldsymbol{x},t)$ and $p_{\mathrm{O}}(\boldsymbol{x},t)$ is carried out in an intermediate region, based on the method of matched asymptotic expansions. An intermediate variable is defined by

$$\xi_i = M^{\alpha} x_i', \quad \xi = M^{\alpha} x' \quad (0 < \alpha < 1).$$

In terms of ξ, the inner and outer variables x' and $\hat{x}$ are written as $x' = M^{-\alpha}\xi$, $\hat{x} = M^{1-\alpha}\xi$. Thus in the limit of $M \to 0$ with a fixed ξ, we have $x' \to \infty$ and $\hat{x} \to 0$.

Since we are interested here in the leading terms, the matching principle is

$$\lim_{M\to 0} p'(\boldsymbol{x}' = M^{-\alpha}\xi, t', M) = \lim_{M\to 0} \hat{p}(\boldsymbol{x} = M^{1-\alpha}\xi, t', M), \tag{3.11}$$

with ξ fixed, where p' and $\hat{p}$ are the leading-order expressions in each region. This permits determination of the functions $A_0, A_i, A_{ij}, \dots$ in terms of $\boldsymbol{\omega}(\boldsymbol{x},t)$. This is called 'vortex sound'.

4. Acoustic emission by vortices in free space

4.1. *General description*

We first consider the vortex sound in an unbounded fluid with no solid body. The Green function in free space is given by

$$G(\boldsymbol{x},\boldsymbol{y}) = \frac{1}{4\pi|\boldsymbol{x}-\boldsymbol{y}|}. \tag{4.1}$$

This is substituted in the inner solution (3.9), in which the magnitude of $\boldsymbol{y}$ is $y = O(l)$. The matching procedure demands the expression at large distances $x \gg y$. Using the expansion (2.9) and applying the operator ∇_y to G, one finds

$$\nabla_y G(\boldsymbol{x},\boldsymbol{y}) = -\frac{1}{4\pi}\nabla\frac{1}{x} + \nabla_y \times \boldsymbol{g} + O(x^{-4}), \tag{4.2}$$

where

$$\boldsymbol{g} = \frac{1}{4\pi x^5}(\boldsymbol{x}\cdot\boldsymbol{y})(\boldsymbol{x}\times\boldsymbol{y}). \tag{4.3}$$

In order to obtain the second term, we have used the relation

$$\nabla_y \times \boldsymbol{g} = \frac{1}{4\pi x^5}(3\boldsymbol{x}(\boldsymbol{x}\cdot\boldsymbol{y}) - x^2\boldsymbol{y}) = \frac{1}{4\pi} y_j \frac{\partial^2}{\partial x_i\,\partial x_j}\frac{1}{x} = \nabla_y \Phi_2, \tag{4.4}$$

where

$$\Phi_2 = a_{ij} y_i y_j, \quad a_{ij} = \frac{1}{8\pi}\frac{\partial^2}{\partial x_i\,\partial x_j}\frac{1}{x}.$$

It is interesting to find that the vector $\boldsymbol{g}$ is a vector potential of the flow corresponding to the velocity potential $\Phi_2(\boldsymbol{y})$, which represents a stagnation-point flow for a fixed $\boldsymbol{x}$. When (4.2) is substituted into (3.9), it is readily seen that the contribution from the first term disappears. Regarding the second term, partial integration transforms the integrand into the form $-\rho_0(\nabla\times\boldsymbol{L})\cdot\boldsymbol{g}$. From (3.2), we have $\nabla\times\boldsymbol{L}=\nabla\times(\boldsymbol{\omega}\times\boldsymbol{v})$, which is equal to $-\partial\boldsymbol{\omega}/\partial t$, from (3.3). Thus the inner pressure (3.9) is reduced to the expression

$$p_{\mathrm{I}}(\boldsymbol{x},t)=\rho_0\frac{\mathrm{d}}{\mathrm{d}t}\int\boldsymbol{\omega}(\boldsymbol{y},t)\cdot\boldsymbol{g}(\boldsymbol{x},\boldsymbol{y})\,\mathrm{d}^3y+O(x^{-4}), \tag{4.5}$$

neglecting terms of $O(M^2)$ since this is derived from (3.1). Owing to the identity $\boldsymbol{\omega}\cdot(\boldsymbol{x}\times\boldsymbol{y})=\boldsymbol{x}\cdot(\boldsymbol{y}\times\boldsymbol{\omega})$, this is transformed to

$$p_{\mathrm{I}}(\boldsymbol{x},t)=\rho_0\dot{Q}_{ij}(t)\frac{\partial^2}{\partial x_i\,\partial x_j}\frac{1}{x}+O(x^{-4}), \tag{4.6}$$

where the tensor Q_{ij} is defined in (2.11) and the dot denotes differentiation with respect to the time t. In order to derive the last expression, we have used the relation

$$3Q_{ij}\frac{x_ix_j}{x^5}=Q_{ij}\left(\frac{3x_ix_j}{x^5}-\frac{\delta_{ij}}{x^3}\right)=Q_{ij}\frac{\partial^2}{\partial x_i\,\partial x_j}\frac{1}{x},$$

since $Q_{ii}=0$. Given the vorticity field $\boldsymbol{\omega}(\boldsymbol{x},t)$, the tensor $Q_{ij}(t)$ is expressed as a function of t, and then (4.6) represents the asymptotic form of $p_{\mathrm{I}}(\boldsymbol{x},t)$ as $x\to\infty$. It is remarkable that the leading term is characterized by the quadrupole potentials $(\partial^2/\partial x_i\,\partial x_j)x^{-1}$ with the time-dependent coefficients $\dot{Q}_{ij}(t)$ (Obermeier 1976). It is interesting to find that the pressure (4.6) is obtained from (2.11) using the relation $p=-\rho_0\,\partial\Phi/\partial t$ (for the linear irrotational perturbation) since the fluid impulses P_i are conserved in the free-space problem (Kambe & Minolta 1981).

In terms of the inner variables

$$p'=\dot{Q}'_{ij}\frac{\partial^2}{\partial x'_i\,\partial x'_j}\frac{1}{x'}+O(M^2). \tag{4.7}$$

The matching principle suggests that

$$\hat{A}_{ij}=M^3\dot{Q}'_{ij}\quad\left(A_{ij}=M^3\frac{\rho_0}{l^3}\dot{Q}_{ij}(t)\text{ in the dimensional form}\right), \tag{4.8}$$

the other coefficients being the higher orders. (There is an ambiguity in the matching to determine the monopole term, which is resolved by a higher-order matching, Crow 1970; Obermeier 1976.) Thus we find from (3.10) and $M=l/\lambda$ that the external solution is given by

$$p_{\mathrm{O}}(\boldsymbol{x},t)=\rho_0\frac{\partial^2}{\partial x_i\,\partial x_j}\frac{\dot{Q}_{ij}(t-x/c)}{x} \tag{4.9}$$

to leading order. This is the pressure formula of the vortex sound. Equation (4.9) shows that the fluctuation of $Q_{ij}(t)$ propagates to the outer space as a quadrupole wave.

In the far field as $\hat{x}\to\infty$, only the space derivative applied to the retarded time becomes dominant, and the pressure takes the simpler form

$$p_{\mathrm{F}}=\frac{\rho_0}{c^2}\frac{x_ix_j}{x^3}\ddot{Q}_{ij}\left(t-\frac{x}{c}\right) \tag{4.10}$$

(Möhring 1978). The tensor coefficient Q_{ij} is to be evaluated at the retarded time $t-x/c$.

In order to estimate the scaling law, we use the length l and the velocity u as reference. Then the time t and the tensor Q_{ij} are normalized by l/u and l^4u. Thus we find the scaling law

$$p_{\mathrm{F}}^{(\mathrm{q})} \sim \frac{\rho_0 u^4}{c^2}\frac{l}{x} = \rho_0 u^2 M^2 \frac{l}{x}. \tag{4.11}$$

In the linear theory of sound, the particle velocity corresponding to p_{F} is given by $v_{\mathrm{F}} = p_{\mathrm{F}}/\rho_0 c$. Hence,

$$v_{\mathrm{F}}^{(\mathrm{q})} \sim uM^3 \frac{l}{x}.$$

The sound intensity I is given by $p_{\mathrm{F}}^2/\rho_0 c$. This leads to the well-known intensity law (Lighthill 1952):

$$I \sim \rho_0 u^3 M^5 \frac{l^2}{x^2} \propto u^8.$$

4.2. *Acoustic emission by loop vortices*

The pressure formula (4.5) permits the following interpretation. Suppose that there exist n (unlinked) vortex tubes and all the vortex lines are included in them. The centreline of each vortex tube is denoted by a closed curve C_k ($k = 1, \ldots, n$): namely we consider a system of n vortex rings.

On the assumption that the vortex tube is very thin and the vorticity is uniformly distributed over its cross-section, the strength Γ_k of the kth vortex is given by $|\boldsymbol{\omega}(k)|\,\sigma_k$ where σ_k is the cross-section area. Writing a line element of C_k as $\mathrm{d}\boldsymbol{s}(k)$, we have $\boldsymbol{\omega}\,\mathrm{d}^3\boldsymbol{y}(k) = |\boldsymbol{\omega}|\,\sigma_k\,\mathrm{d}\boldsymbol{s}(k) = \Gamma_k\,\mathrm{d}\boldsymbol{s}(k)$. Then the integral in (4.5) is

$$\int \boldsymbol{\omega}\cdot\boldsymbol{g}\,\mathrm{d}^3\boldsymbol{y} = \sum_{k=1}^{n} \Gamma_k \oint_{C_k} \boldsymbol{g}\cdot\mathrm{d}\boldsymbol{s} = \sum_k \Gamma_k \int_{S_k} (\nabla\times\boldsymbol{g})\cdot\boldsymbol{n}\,\mathrm{d}S \tag{4.12}$$

by the Stokes theorem, where S_k is an open surface with its circumference bounded by the curve C_k. As noted in the previous section, $\nabla\times\boldsymbol{g}$ represents the velocity of a stagnation-point flow of velocity potential Φ_2. Thus it is found from (4.5) that the pressure p_{I} is given by the time derivative of the sum of the volume flux of the flow Φ_2 through the vortex loop C_k multiplied by $\rho_0\Gamma_k$.

Using (4.4), we have an alternative expression

$$p_{\mathrm{I}} = \frac{\rho_0}{4\pi}\sum_k \Gamma_k \dot{J}_{ij}(k)\frac{\partial^2}{\partial x_i\,\partial x_j}\frac{1}{x}, \tag{4.13}$$

where the summation with respect to $i,j = 1,2,3$ is understood (following the summation convention), and the surface integral

$$J_{ij}(k) = \int_{S_k} y_i\,n_j\,\mathrm{d}S \tag{4.14}$$

depends on t. It can be shown that this is equivalent to (4.6) by noting that

$$Q_{ij} = \frac{1}{4\pi}\sum_k \Gamma_k(J_{ij} - \tfrac{1}{3}\delta_{ij}J_{mm}), \quad \delta_{ij}\frac{\partial^2}{\partial x_i\,\partial x_j}\frac{1}{x} = 0 \quad (x \neq 0).$$

The same argument as in the previous section leads to the far-field expression

$$p_{\mathrm{F}} = \frac{\rho_0}{4\pi c^2}\frac{1}{x}e_i e_j \sum_k \Gamma_k[\dddot{J}_{ij}(k) - \tfrac{1}{3}\delta_{ij}\dddot{J}_{mm}(k)] = \frac{\rho_0}{8\pi c^2}\frac{1}{x}\sum_k \Gamma_k \dddot{J}(k,\boldsymbol{e}), \tag{4.15}$$

where $e_i = x_i/x$, and

$$J(k,\boldsymbol{e}) \equiv 2e_i e_j[J_{ij}(k) - \tfrac{1}{3}\delta_{ij}J_{mm}(k)] = -\int_{S_k} n_j \frac{\partial}{\partial y_j}\Phi_*\,\mathrm{d}S,$$

with $\Phi_* = \frac{1}{3}y_i^2 - e_i e_j y_i y_j$. Thus the far-field pressure is related to the third time derivative of the volume flux $J(k, \boldsymbol{e})$ through C_k of the potential flow Φ_*, which is a stagnation-point flow from the direction $\boldsymbol{e}$ ($= \boldsymbol{x}/x$) to the origin.

4.3. *Head-on collision of two vortex rings*

Axisymmetric collision of two circular vortex rings presents a particularly simple example of the acoustic emission. This configuration can be realized in the laboratory (see §4.4).

Suppose that we have two vortex rings having a common symmetry axis x_3, with the one vortex being a mirror image of the other with respect to the plane $x_3 = 0$ (thus the strengths are opposite), and that they approach each other according to the equation of motion. The distance of the vortex centre from the symmetry plane is denoted by Z. The vortex ring is characterized here by its strength Γ, ring radius R and the radius δ_c of its thin vortex core. The translation velocity U in a single state ($R = R_0$ and $\delta_c = \delta_0$) is assumed to be given by Kelvin's formula

$$U = \frac{\Gamma}{4\pi R_0}\left(\log\frac{8R_0}{\delta_0} - \frac{1}{4}\right).$$

The axisymmetric configuration of two vortex rings (the vortex strength on the positive side being $-\Gamma$ with $\Gamma > 0$) yields

$$Q_{ij} = 0 \quad (i \neq j),$$

$$Q_{11} = Q_{22} = -\tfrac{1}{2}Q_{33} = -\tfrac{1}{12}Q(t),$$

that is, the tensor Q_{ij} is represented in terms of one scalar function $Q(t) = -2\Gamma R^2(t)\, Z(t)$. The interacting motion of two vortex rings is described by a system of differential equations (Kambe & Minota 1983), originally derived by Dyson (1893). It is interesting to find that the quantity $-R^2Z$ is the value of the Stokes stream function at the vortex core (Z, R) of an axisymmetric stagnation-point flow toward the plane $x_3 = 0$ (from both sides). Therefore Q represents the volume flux through the two vortex rings, multiplied by Γ.

Introducing these into (4.10) one obtains

$$p_F = \frac{\rho_0}{4c^2}\ddot{Q}\left(t - \frac{x}{c}\right)\frac{1}{x}(\cos^2\theta - \tfrac{1}{3}). \tag{4.16}$$

The factor $\ddot{Q}(t)$ represents the wave profile, whereas the factor $(\cos^2\theta - \frac{1}{3})$ gives the quadrupolar distribution, where the angle θ denotes $\cos^{-1}(x_3/x)$ for the observation point $\boldsymbol{x}$.

4.4. *Laboratory experiment*

Apparatus to make a vortex ring, using a shock tube, has been described fully: Kambe & Minota 1983; Kambe, Minota & Ikushima 1985. When a shock wave emerges a straight nozzle, a vortex ring is formed on exit by the shock impulse. Two straight nozzles are set to face each other with a common axis in a cubic anechoic chamber. The two vortices, formed simultaneously at each nozzle exit, approach each other with their self-induced motion, and they collide at a central position (figure 2). When the vortices approach the mid-plane of collision, their radii increase rapidly and the vortex cores come into contact. At the same time their forward motion is blocked, and then the two vortices are broken down.

The acoustic waves generated by the vortex collision were detected by four microphones placed in the far field (Minota & Kambe 1986). In view of the

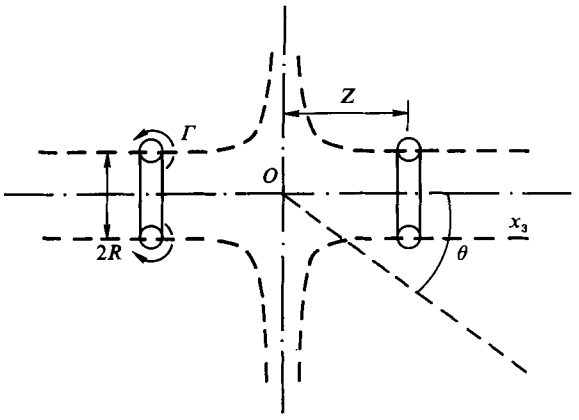

FIGURE 2. Head-on collision of two vortex rings (definition sketch).

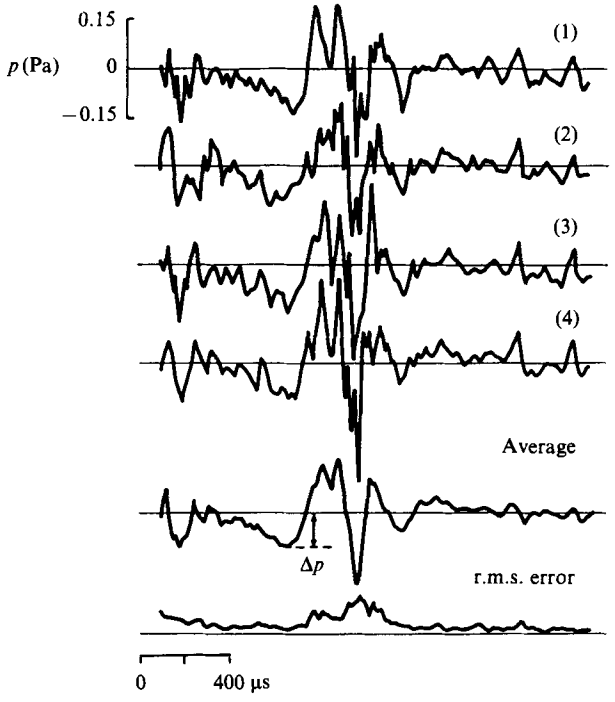

FIGURE 3. Example of four pressure signals (curves 1–4) detected at $\theta = 170°$ and $x = 630$ mm, and the average and r.m.s. error of ten such signals at each time point ($U = 34$ m/s, $R_0 = 4.7$ mm).

axisymmetric configuration, the microphone position is placed at an angle θ to the nozzle axis. The detected signals are processed by digital methods. The test procedure and the extraction method for the wave profile imbedded in the original noisy signal are as described in Kambe *et al.* (1985). The extracted signals are averaged over ten data sets. Curves (1–4) in figure 3 are examples of the wave profiles before the averaging, and at the bottom the averaged profile (over ten such curves) is shown together with its r.m.s. error at each time point.

Figure 4 shows a perspective diagram of the average-pressure profile $p_m(t)+p_q(t)(1-3\cos^2\theta)$ (see below) observed in the experiment. The radial co-

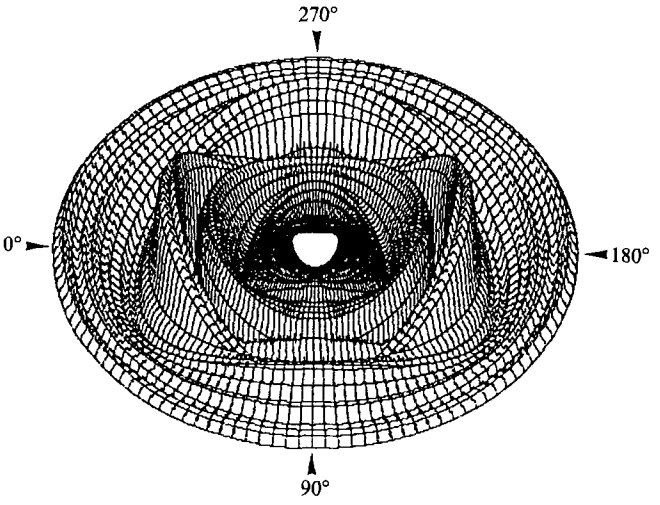

FIGURE 4. Perspective diagram of the observed acoustic pressure (maximum amplitude being about 0.15 Pa): $U = 33$ m/s, $R_0 = 4.7$ mm, $x = 630$ mm. Equal times are shown by concentric circles, the outer one being earlier in time.

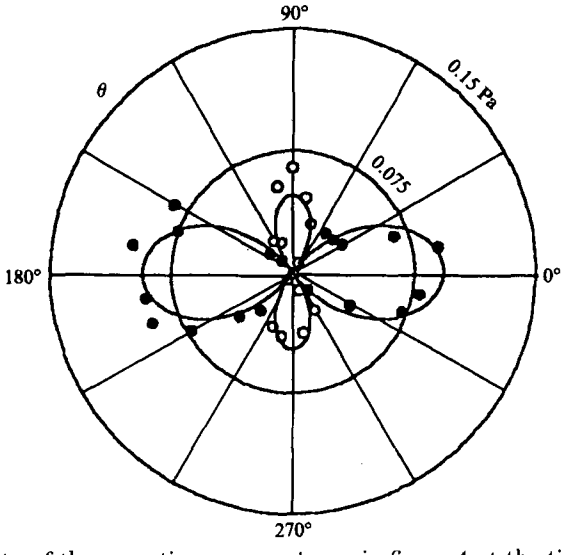

FIGURE 5. Directivity of the acoustic pressure shown in figure 4 at the time corresponding to the first (arrowed) peak of the profile of figure 6.

ordinate is the time, with the outer concentric circle being earlier in time. The height denotes the acoustic pressure. The initial velocity U and radius R_0 were 33 m/s and 4.7 mm respectively, and the wave was observed at $x = 630$ mm.

An instantaneous directivity of the radiation is shown in figure 5, in which the radial length from the origin represents the magnitude of pressure on a linear scale. The filled and open circles respectively denote negative and positive values of the observed pressure. The solid curve shows the sum of two main components: a quadrupole $p_q(1-3\cos^2\theta)$ and a monopole p_m (independent of θ), where the coefficients p_q and p_m were determined from a truncated Fourier decomposition of the profile at the given time. (The series truncation is necessary since the signals were

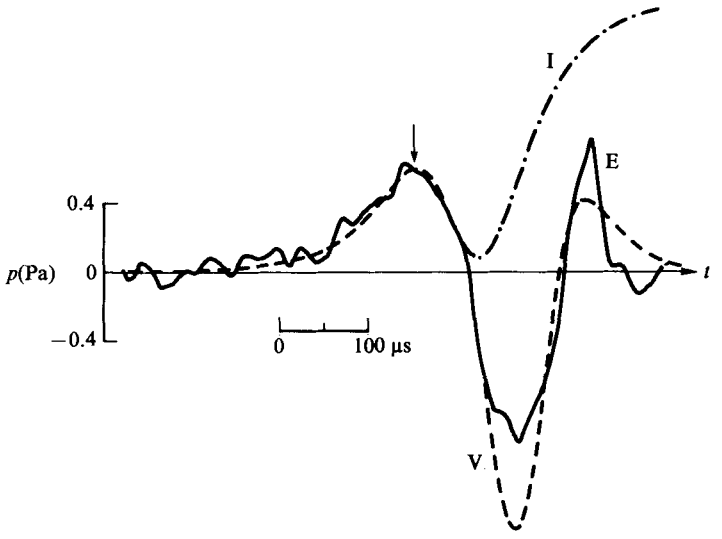

FIGURE 6. Comparison between three pressure profiles of the quadrupole coefficient $p_q(t)$: observation (——), an inviscid vortex model (—·—·—·) and a viscous vortex model (– – –). $U = 57$ m/s, $R_0 = 5.4$ mm, $x = 500$ mm.

obtained at every 10° angular position.) The four-lobe curve shows the quadrupole nature of the emission.

Figure 6 shows a comparison between three pressure profiles of $p_q(t)$ of the quadrupolar component $p_q(t)(1-3\cos^2\theta)$: observation (solid, E), an inviscid vortex motion (chain dotted, I) and a model taking account of the viscosity (broken, V). The inviscid theory considered above gives the curve I. It is inferred from this figure that the viscous effect becomes important in the final period. (Recently K. Shariff 1986, private communication, has shown by numerical analysis that the pressure dip, which cannot be obtained (in the curve I) by Dyson's equation of vortex motion for very thin circular cores, can be predicted by an inviscid theory taking account of the finite size of the cores and their deformation at the collision.) The curve E is obtained from Fourier decomposition of the detected signals, which also includes a significant isotropic component (Kambe & Minota 1983; Minota & Kambe 1986). The generation of an isotropic monopolar component by a viscosity effect is discussed in Kambe (1984) and Obermeier (1985).

5. Acoustic emission from vortex–body interaction

5.1. *General description*

When there is a solid body in the vicinity of the vortex motion, the wavefield is characterized by a dipole radiation rather than the quadrupole in the previous free-space problem. The boundary condition to be satisfied on the body surface causes the more powerful emission of waves of a dipole nature. The fluctuating pressure over the body surface results in a fluctuating net force acting on the body. Conversely the fluctuating force, multiplied by a minus sign, is equivalent to the rate of change of the resultant momentum of the fluid system.

The Green function in the presence of a solid body of size $O(l)$ near the origin is represented approximately by

$$G_{\mathrm{B}}(\boldsymbol{x},\boldsymbol{y}) = \frac{1}{4\pi|\boldsymbol{x}-\boldsymbol{Y}(\boldsymbol{y})|}. \tag{5.1}$$

where

$$\boldsymbol{Y}(\boldsymbol{y}) = \boldsymbol{y}+\boldsymbol{\Phi}(\boldsymbol{y}). \tag{5.2}$$

This is valid when $\boldsymbol{x}$ is far from the body, i.e. $|\boldsymbol{x}| \gg l$ (Howe 1975*a*, Obermeier 1980). The vector function $Y_i(\boldsymbol{x})$ denotes the velocity potential ($\nabla^2 Y_i = 0$) of a hypothetical flow around the body with a unit velocity to the y_i direction at infinity ($i = 1,2,3$). The first term y_i represents the uniform flow of a unit velocity and the vector function $\boldsymbol{\Phi}_i(\boldsymbol{y})$ represents a correction due to the presence of a body, which imposes the boundary condition of vanishing normal velocity. When there is no solid body, one may put $\boldsymbol{\Phi}_i = 0$. Then (5.1) reduces to (4.1).

The function $G_{\mathrm{B}}(\boldsymbol{x},\boldsymbol{y})$ satisfies the boundary condition on the body surface S, that is

$$\boldsymbol{n}\cdot\nabla_y G_{\mathrm{B}} = 0 \quad \text{for } \boldsymbol{y} \text{ on } S.$$

This is verified by differentiating (5.1) with respect to y_i

$$\nabla_y G_{\mathrm{B}} = \frac{(x_i - Y_i)\,\nabla_y Y_i}{4\pi|\boldsymbol{x}-\boldsymbol{Y}|^3}, \tag{5.3}$$

and using the property $\boldsymbol{n}\cdot\nabla Y_i = 0$ for $\boldsymbol{y}$ on S, since ∇Y_i denotes the velocity of a potential flow around the body. It is readily seen that the singularity of the function G_{B} tends to the correct behaviour as x/l, $y/l \to \infty$, since we have $|\boldsymbol{\Phi}(\boldsymbol{y})| = O(y^{-2})$ for a compact body of size $O(l)$ and therefore G_{B} tends to $1/[4\pi|\boldsymbol{x}-\boldsymbol{y}|]$. The Green function G must satisfy the equation $\nabla^2 G = 0$ when restricted to the case $|\boldsymbol{x}| \gg |\boldsymbol{y}|$. Using $|\boldsymbol{x}| \gg |\boldsymbol{y}|$ in (5.1), we develop it in a form similar to (2.9), but using Y_i in place of y_i and apply the operator ∇_y^2. Then, the first two terms disappear (since $\nabla^2 Y_i = 0$), and the third term gives

$$\nabla_y^2 G_{\mathrm{B}} = \frac{1}{8\pi}\nabla_y^2(Y_i\,Y_j)\frac{\partial^2}{\partial x_i\,\partial x_j}\frac{1}{x} + O(x^{-4}) = O(x^{-3}).$$

Therefore the function G_{B} satisfies the equation $\nabla^2 G = 0$ within an error of $O(x^{-3})$. However the term of $\nabla_y G_{\mathrm{B}}$ to be used in the following is a lower-order term of $O(x^{-2})$ ((5.4) below); thus G_{B} has the correct behaviour up to that order. This permits the use of (5.1) as the Green function in the present context.

Using an asymptotic expansion of the form (2.9), (5.3) is written as

$$\nabla_y G_{\mathrm{B}} = \frac{x_i}{4\pi x^3}\nabla_y Y_i + O(x^{-3}). \tag{5.4}$$

The velocity field of the potential flow represented by $\nabla_y Y_i$ is incompressible. This permits introduction of a vector potential $\boldsymbol{\Psi}_i$ (a vector for each $i = 1,2,3$) by the relation

$$\nabla Y_i = \nabla\times\boldsymbol{\Psi}_i, \quad \operatorname{div}\boldsymbol{\Psi}_i = 0 \quad (i = 1,2,3). \tag{5.5}$$

In cases of two dimension or axisymmetry, the vector $\boldsymbol{\Psi}_i$ is related to the stream function. Since $\nabla\times(\nabla\times\boldsymbol{\Psi}_i) = -\nabla^2\boldsymbol{\Psi}_i = 0$ (i.e. each component of $\boldsymbol{\Psi}_i$ is harmonic), we may choose that $\boldsymbol{\Psi}_i = 0$ on S without violating (5.5). Using (5.4) and (5.5) in (3.9), one obtains

$$p_{\mathrm{I}}(\boldsymbol{x},t) = -\frac{\rho_0}{4\pi}\frac{x_i}{x^3}\int \boldsymbol{L}\cdot(\nabla_y\times\boldsymbol{\Psi}_i)\,\mathrm{d}^3\boldsymbol{y}. \tag{5.6}$$

Integrating by parts and using (3.2) and (3.3) as in the previous case when we obtained (4.5), one finds

$$p_{\mathrm{I}}(\boldsymbol{x},t) = -\frac{\rho_0}{4\pi}\dot{\Pi}_i \frac{\partial}{\partial x_i}\frac{1}{x} + O(x^{-3}), \tag{5.7}$$

where

$$\Pi_i(t) = \int \boldsymbol{\omega}\cdot\boldsymbol{\Psi}_i \,\mathrm{d}^3\boldsymbol{y}. \tag{5.8}$$

Thus we have found that the inner pressure tends to the form of a dipole potential at large distances in contrast to the previous case of a quadrupole.

In terms of the inner variables

$$p'(\boldsymbol{x}',t) = -\frac{1}{4\pi}\dot{\Pi}'_i \frac{\partial}{\partial x'_i}\frac{1}{x'},$$

where $\dot{\Pi}'_i = \dot{\Pi}_i/u^2l^2$. The matching principle suggests that

$$\hat{A}_i = -M^2\frac{1}{4\pi}\dot{\Pi}'_i \quad \left(A_i = -\frac{M^2\rho_0}{4\pi l^2}\dot{\Pi}_i(t) \quad \text{in the dimensional form}\right),$$

the other coefficients being of higher order in M. Thus the acoustic pressure in the outer region is given by

$$p_{\mathrm{O}} = -\frac{\rho_0}{4\pi}\frac{\partial}{\partial x_i}\frac{\Pi_i(t-x/c)}{x}. \tag{5.9}$$

In the far field $\hat{x}\to\infty$, this reduces to

$$p_{\mathrm{F}} = \frac{\rho_0}{4\pi c}\ddot{\Pi}_i\left(t-\frac{x}{c}\right)\frac{x_i}{x^2}. \tag{5.10}$$

In order to obtain the scaling law, we note that Π_i is normalized by ul^3. Therefore using the order estimate of $O(\partial/\partial t) = u/l$, we find the scaling law for the dipole emission,

$$p^{(\mathrm{d})} \sim \frac{\rho_0 u^3}{c}\frac{l}{x} = \rho_0 u^2 M\frac{l}{x}. \tag{5.11}$$

The corresponding velocity is

$$v_{\mathrm{F}}^{(\mathrm{d})} \sim uM^2\frac{l}{x}.$$

5.2. *Acoustic emission by a loop vortex*

As in §4.2, suppose that there exists a vortex tube forming a closed loop, of which the centreline is denoted by a closed curve C. Writing a line element of C as $\mathrm{d}\boldsymbol{s}$, (5.8) is written as

$$\Pi_i(t) = \Gamma\oint_C \boldsymbol{\Psi}_i\cdot\mathrm{d}\boldsymbol{s} = \Gamma\int_S (\nabla\times\boldsymbol{\Psi}_i)\cdot\boldsymbol{n}\,\mathrm{d}S, \tag{5.12}$$

where S is an open surface with the circumference bounded by the curve C, and $\nabla\times\boldsymbol{\Psi}_i$ represents the velocity of a hypothetical potential flow around the body. Therefore, Π_i is equal to the volume flux J_i of the flow $\nabla\times\boldsymbol{\Psi}_i$ through the closed curve C, multiplied by Γ:

$$\Pi_i(t) = \Gamma J_i(t),$$

where

$$J_i = \int_S (\nabla\times\boldsymbol{\Psi}_i)\cdot\boldsymbol{n}\,\mathrm{d}S. \tag{5.13}$$

The volume flux J_i depends on the vortex position. Although the potential flow $\nabla\times\boldsymbol{\Psi}_i$ is steady, the flux J_i is time dependent because the vortex position (the position of C) changes.

Thus we have found the following law: when a vortex ring (not necessarily circular)

moves near a solid body, the flux J_i through the vortex loop C changes with time, which causes sound emission according to (5.10):

$$p_{\mathrm{F}} = \frac{\rho_0 \Gamma}{4\pi c} \dot{J}_i\left(t - \frac{x}{c}\right) \frac{x_i}{x} \frac{1}{x}. \tag{5.14}$$

This phenomenon is similar to Faraday's law in the theory of electromagnetism. However the present case of vortex sound is valid in an asymptotic sense in the limit $M \to 0$.

5.3. *Force on the body*

It is interesting to know that the coefficient function Π_i is related to the resultant force $F_i(t)$ on the body. Curle (1955) showed, in the same situation as in §5.1, that the sound pressure in the far field is given by

$$p_{\mathrm{O}} = \frac{1}{4\pi} \frac{\partial}{\partial x_i} \frac{F_i(t - x/c)}{x}. \tag{5.15}$$

According to the fundamental law of mechanics, a body acts on the fluid system with the force $-F_i$. Thus (5.15) shows that the force acting on the fluid generates an acoustic wave of dipole type. Equations (5.15) and (5.9) suggest the relation

$$\left.\begin{aligned} \rho_0 \dot{\Pi}_i(t) &= -F_i(t), \\ \text{therefore} \qquad F_i &= -\rho_0 \Gamma \dot{J}_i. \end{aligned}\right\} \tag{5.16}$$

Thus it is found that the force on the body is related to the volume flux through the vortex loop.

In order to obtain (5.9) we used the volume integrals (3.9) and (5.8) with the help of the Green function (5.1). On the other hand, the formula (5.15) was derived from a surface integral, with F_i being the surface integral of the stress over the solid body. Both integrals are combined in (5.16).

By linear perturbation theory, the pressure p and the velocity potential Φ are related by $p = -\rho_0 \partial\Phi/\partial t$. Far from the eddy region, the velocity decays like x^{-3} and diminishes at large distances, where linear theory may be applied. Using the pressure (5.7), we find that the velocity potential Φ for the inner flow takes the form of the dipole potential:

$$\Phi = \frac{1}{4\pi} \Pi_i \frac{\partial}{\partial x_i} \frac{1}{x} + O(x^{-3}).$$

It is verified for axisymmetric cases (Miyazaki & Kambe 1986) that the axial force F on the solid body is related to the dipole coefficient A of the velocity potential, defined by $A = -\Pi_3/4\pi$ (only the non-zero component) in the present notation, and connected by the equation $F = 4\pi\rho_0 \, \mathrm{d}A/\mathrm{d}t = -\rho_0 \, \mathrm{d}\Pi_3/\mathrm{d}t$. This is consistent with (5.16).

5.4. *A vortex ring moving near a circular cylinder*

A laboratory experiment has been performed for a circular vortex ring moving near a circular cylinder of comparable cross-section (Kambe, Minota & Ikushima 1986; paper in preparation by T. Minota & T. Kambe). The vortex travels along a nearly straight line. In the absence of a solid body a vortex travelling with a constant velocity is silent. However the presence of a body leads to the generation of an acoustic wave of dipole nature, as is considered in §5.3. However observation shows that the dipole axis rotates in the present case, which is seen in the diagram on the left-hand side of figure 7. This is because the force vector acting on the cylinder changes direction as the vortex moves relatively to the cylinder.

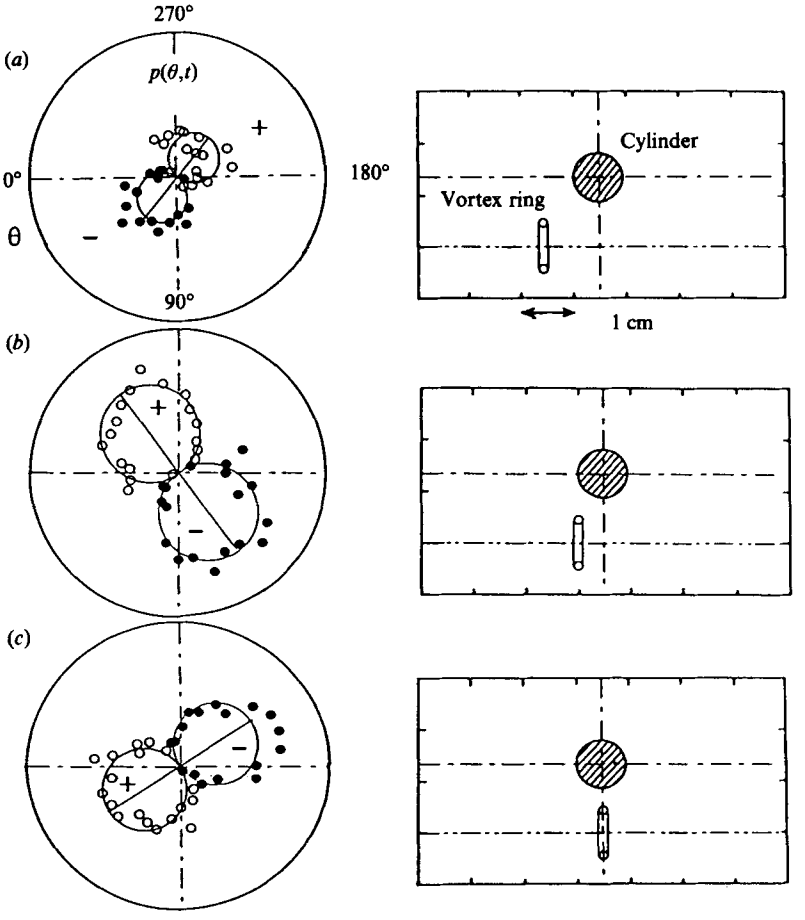

FIGURE 7. Vortex position relative to the circular cylinder (right) and the corresponding pressure distribution in the far field (left) where the outer circle corresponds to 0.08 Pa: $U = 27$ m/s, $R_0 = 4.7$ mm. (*a*) $t = 1695$ μs; (*b*) 1905 μs; (*c*) 2100 μs.

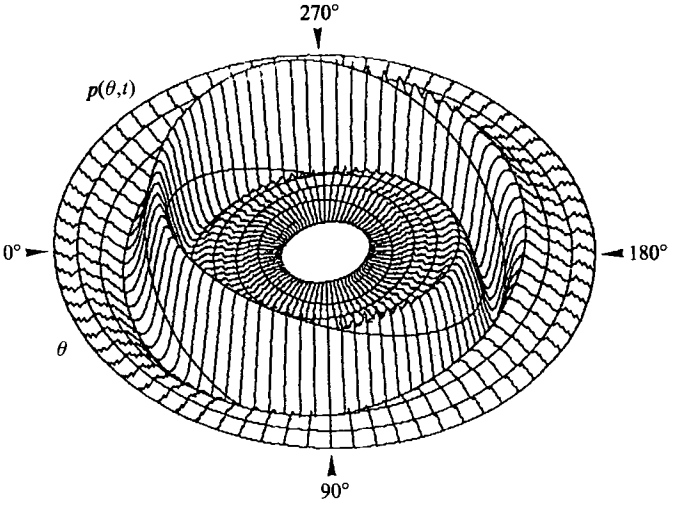

FIGURE 8. Perspective plot of the pressure using the same data as in figure 7.

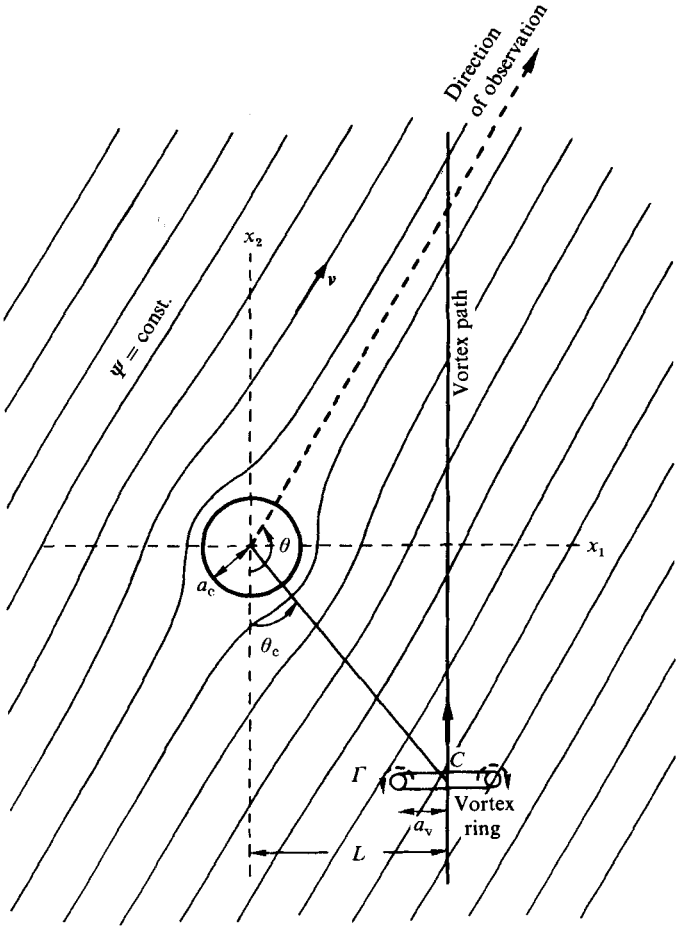

FIGURE 9. Schematic diagram, illustrating the theory with Ψ = const. denoting the streamlines.

In the polar diagram of figure 7 (left), the radial coordinate denotes the pressure observed in the far field (with a linear scale), the outer circle corresponding to 0.08 Pa. The open and filled circles respectively denote positive and negative values of the observations. The translation velocity U and radius R_0 of the vortex ring are 27 m/s and 4.7 mm respectively. The corresponding position of the vortex is shown on the right-hand diagram (shifted back by the retarded time) together with the time from an experimentally fixed origin. Figure 8 shows a perspective plot of the pressure. The spiral structure corresponds to the rotation of the dipole axis. Figure 9 shows a diagram in the plane (x_1, x_2) perpendicular to the cylinder axis x_3, in which the cross-section of the cylinder is shown at the centre and streamlines of a hypothetical potential flow around it are depicted in addition to the schematic plot of a vortex ring and its straight-line path. In this case the vector potential $\boldsymbol{\Psi}_i$ is given in the form $(0, 0, \Psi_i)$ $(i = 1, 2)$ where Ψ_i is the stream function of a two-dimensional flow around the cylinder with a unit velocity in the x_i direction at infinity. It is noted that the combination $J_i x_i/x$ in (5.14) denotes the volume flux of a potential flow to the observation direction. The flux J_i can be computed from (5.13). The pressure (5.14) is proportional to

$$f(t) = \frac{J_i x_i}{x} = J_1(t) \sin\theta - J_2(t) \cos\theta, \tag{5.17}$$

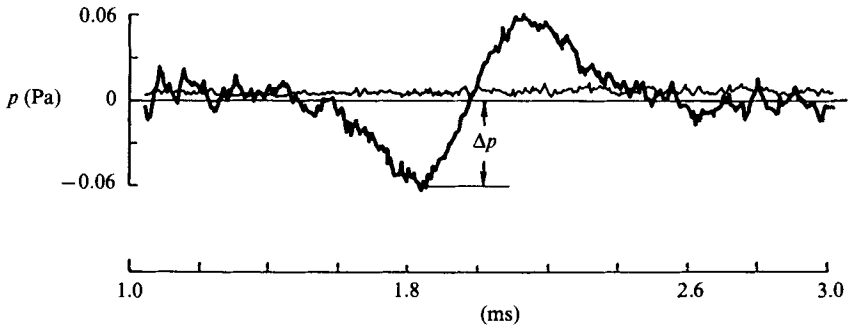

FIGURE 10. An example of an average wave profile (thick) and its r.m.s. error (thin), observed at $\theta = 70°$ and $x = 626$ mm for $U = 28$ m/s, $R_0 = 4.7$ mm, $L = 13.2$ mm and $a_c = 4.5$ mm.

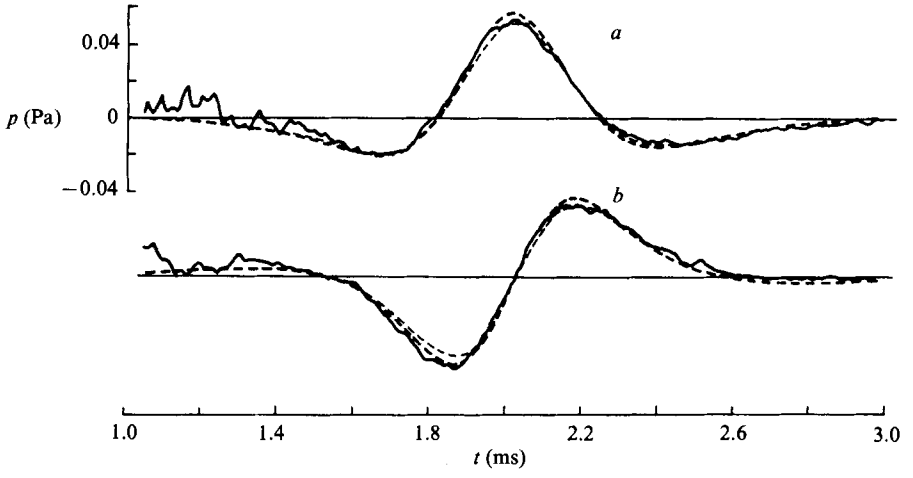

FIGURE 11. Comparison of the dipole coefficients $a(t)$ and $b(t)$: observation (solid) and theoretical profiles computed with $\delta_0/R_0 = 0.15$ (thick broken) and 0.1 (thin broken).

where $x_1/x = \sin\theta$, $x_2/x = -\cos\theta$, with θ denoting the angle measured from the negative x_2 axis.

Figure 10 shows an example of an average wave profile (thick) together with its r.m.s. error (thin) at each time point. The averaged pressure observed at every 10° angular position is decomposed into a Fourier series with respect to θ. It is found that the main component is given in the form

$$p_{\text{obs}}(\theta, t) = a(t)\cos\theta + b(t)\sin\theta, \tag{5.18}$$

in accordance with the expression (5.17), which is characteristic of the dipole emission. The solid curves in figure 11 illustrate experimentally determined profiles $a(t)$ and $b(t)$. Theoretically computed profiles are shown by broken lines for two ratios of the vortex-core radius δ_0 to the ring radius R_0: $\delta_0/R_0 = 0.15$ (thick broken) and 0.1 (thin broken). Agreement in absolute values between the observed and predicted profiles is excellent. This verifies that the wave profile is determined by the second time derivative of the fluxes $J_1(t)$ and $J_2(t)$.

6. Vortex–edge interaction

6.1. *Pressure formula*

When a body is not compact, the wavefields generated by the vortex motion are quite different from the previous two cases. We consider a semi-infinite plate with a sharp edge, near which a vortex ring passes (Kambe *et al.* 1985).

This problem is solved by using the Green function $G_*(\boldsymbol{x}, \boldsymbol{y}; t)$ of the wave equation

$$\left(\frac{1}{c^2}\frac{\partial^2}{\partial t^2} - \nabla^2\right) G_* = \delta(\boldsymbol{x}-\boldsymbol{y})\,\delta(t) \tag{6.1}$$

under the boundary condition (3.7) with the surface S lying in $[x_1 < 0, x_2 = 0, -\infty < x_3 < \infty]$. This Green function has been well studied in the theory of diffraction by a half-plane (Noble 1958; Macdonald 1915) and is reproduced in Ffowcs Williams & Hall (1970), Crighton & Leppington (1970) and Kambe *et al.* (1985).

The acoustic pressure is given directly from the inhomogeneous wave equation (2.5) with (3.2) in the form

$$p_0(\boldsymbol{x}, t) = -\rho_0 \iint \boldsymbol{L}(\boldsymbol{y}, t)\cdot\nabla_y G_*(x, y; t-\tau)\,\mathrm{d}^3\boldsymbol{y}\,\mathrm{d}\tau. \tag{6.2}$$

This is similar in form to (3.9), but with G replaced by G_* and additional time integration added. Although a closed-form solution of G_* is known, it is convenient to use a series form, which leads to a mathematically simple formulation. The assumptions $M \ll 1$ and $l \ll \lambda$ in §1 permit the introduction of the low-frequency Green function (Howe 1975; Kambe *et al.* 1985), which is expressed by the first few terms of a series valid for small l/λ.

In this way, an approximate Green function for the present problem is found to be

$$\nabla_y G_*(\boldsymbol{x}, \boldsymbol{y}; t) = B(\nabla\times\boldsymbol{\Psi})\,\Phi(\boldsymbol{x})\,x^{-\frac{3}{2}}\left(\frac{\mathrm{d}}{\mathrm{d}t}\right)^{\frac{1}{2}}\delta\left(t-\frac{x}{c}\right)\left(1+O\left(\frac{l}{\lambda}\right)\right), \tag{6.3}$$

where

$$\left.\begin{aligned} \boldsymbol{\Psi} &= (0, 0, \Psi(\boldsymbol{y})), \quad B = \frac{1}{(2\pi^3 c)^{\frac{1}{2}}}, \\ \Phi(\boldsymbol{x}) &= X^{\frac{1}{2}}\sin\tfrac{1}{2}\theta, \quad \Psi(\boldsymbol{y}) = -Y^{\frac{1}{2}}\cos\tfrac{1}{2}\theta, \\ X &= (x_1, x_2), \quad Y = (y_1, y_2), \\ \theta &= \tan^{-1}\frac{x_2}{x_1} \quad \text{or} \quad \tan^{-1}\frac{y_2}{y_1}. \end{aligned}\right\} \tag{6.4}$$

Substituting (6.3) into (6.2), performing partial integration and using (3.3), we obtain

$$p(\boldsymbol{x}, t) = \frac{\rho_0}{(2\pi^3)^{\frac{1}{2}}}\frac{\sin\frac{1}{2}\theta\,(\sin\phi)^{\frac{1}{2}}}{c^{\frac{1}{2}}x}\left(\frac{\mathrm{d}}{\mathrm{d}t}\right)^{\frac{3}{2}}\int \boldsymbol{\omega}\cdot\boldsymbol{\Psi}\,\mathrm{d}^3\boldsymbol{y}, \tag{6.5}$$

where $\phi = \cos^{-1}(x_3/x)$. The $\frac{1}{2}$th derivative is defined by

$$\left(\frac{\mathrm{d}}{\mathrm{d}t}\right)^{\frac{1}{2}} g(t) = \frac{1}{2\pi}\int_{-\infty}^{\infty}(-\mathrm{i}\omega)^{\frac{1}{2}}\hat{g}(\omega)\,\mathrm{e}^{-\mathrm{i}\omega t}\,\mathrm{d}\omega = \int_{-\infty}^{t}\dot{g}(s)\,\frac{\mathrm{d}s}{[\pi(t-s)]^{\frac{1}{2}}},$$

depending on the past history, where $(-\mathrm{i})^{\frac{1}{2}} = \exp(-\frac{1}{4}\mathrm{i}\pi)$ and $\hat{g}(\omega)$ is a Fourier coefficient of $g(t)$. Thus it is found that the acoustic pressure is composed of the angular factor

$$F(\theta, \phi) = \sin\tfrac{1}{2}\theta\,(\sin\phi)^{\frac{1}{2}} \tag{6.6}$$

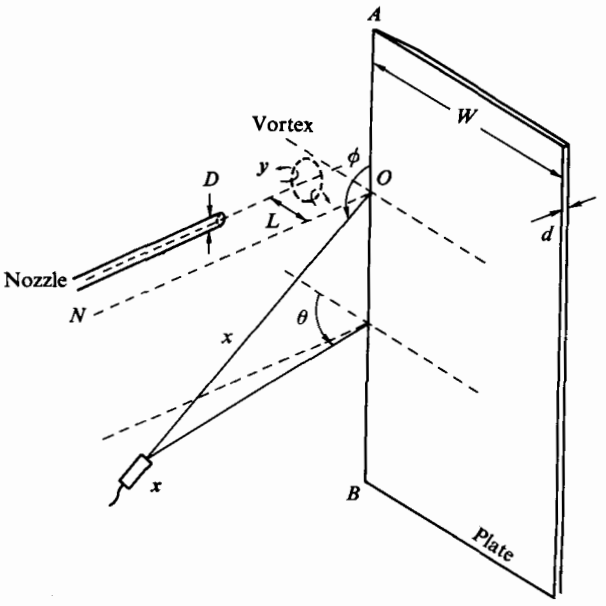

FIGURE 12. Schematic diagram of vortex–edge interaction: $W = 1.0$ m; $d = 5$ mm; D (inner diameter) = 6 mm; vortex radius ≈ 4.7 mm.

and the temporal factor

$$f(t) = \Gamma\left(\frac{\mathrm{d}}{\mathrm{d}t}\right)^{\frac{3}{2}} J(t) \qquad (6.7)$$

with

$$J = \int (\boldsymbol{\nabla} \times \boldsymbol{\Psi}) \cdot \boldsymbol{n} \, \mathrm{d}S.$$

By the same argument as for the normalization, the scaling law for the vortex–edge sound is found as

$$p_{\mathrm{F}}^{(\mathrm{e})} \sim \frac{\rho_0 u^{\frac{5}{2}}}{c^{\frac{1}{2}}} \frac{l}{x} = \rho_0 u^2 M^{\frac{1}{2}} \frac{l}{x}. \qquad (6.8)$$

The corresponding velocity is

$$v_{\mathrm{F}}^{(\mathrm{e})} \sim u M^{1+\frac{1}{2}} \frac{l}{x}.$$

6.2. *A vortex ring passing near the edge*

In a laboratory experiment (Kambe *et al.* 1985) that detected the emission from a vortex ring travelling near the edge of a half-plane along a nearly straight line, both the angular distribution and the temporal profile were found to agree with the predicted profiles $F(\theta, \phi)$ and $f(t)$ with reasonable accuracy. A schematic diagram of the experimental configuration is illustrated in figure 12. Figure 13 shows a polar plot of the pressure $p(\theta, t)$ observed in the plane $\phi = 90°$ at fixed x and t. The radial coordinate is the pressure on a linear scale in Pa. The open and filled circles respectively denote negative and positive values. The observed pressure $p(\theta, t)$ is decomposed into a truncated Fourier series, and it is found that the main component is given by

$$p_* = a_*(t) \sin \tfrac{1}{2}\theta,$$

in accordance with (6.5). The solid curve in figure 13 shows this component at the corresponding time. Note that a curve with the radial distance given by $\sin^2 \frac{1}{2}\theta$ is the cardioid.

Figure 14 is a perspective diagram of the pressure profile observed in the plane

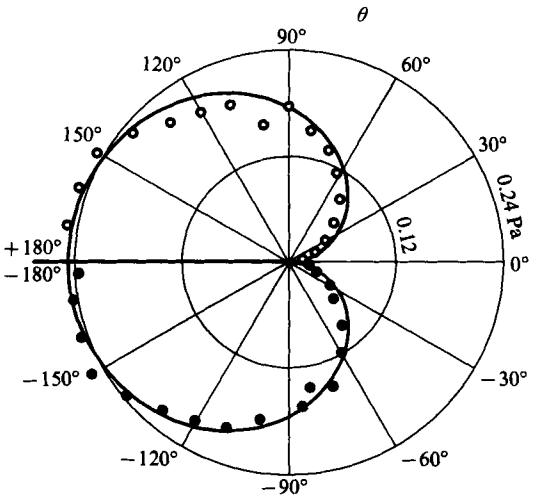

FIGURE 13. Polar plot of the far-field pressure observed at fixed x and t. The solid curve shows the component $a_*(t)\sin\frac{1}{2}\theta$ at the same t.

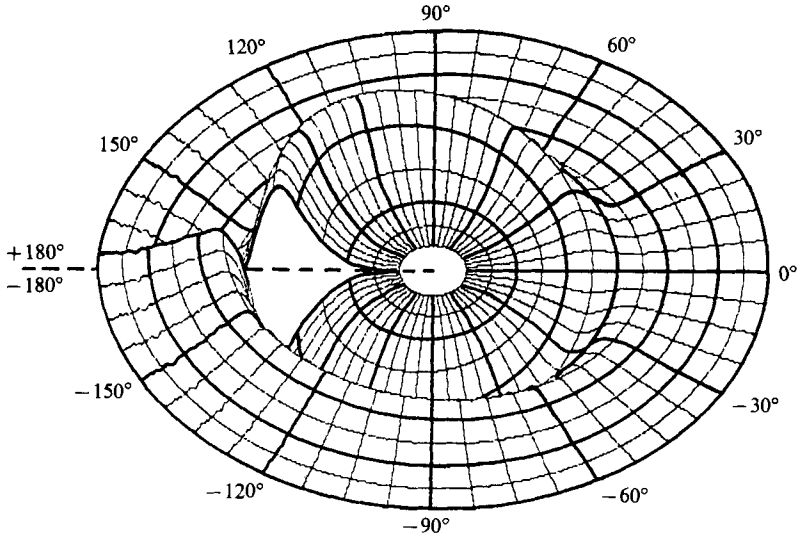

FIGURE 14. Perspective profile of the wave $a_*(t)\sin\frac{1}{2}\theta$. Equal time is shown by the concentric circles.

$\phi = 90°$, the radial coordinate being the time. The half-plane lies at $\theta = \pm 180°$, on each side of which the pressure takes opposite signs. The vortex moved from the positive to negative y_2 axis with the translation speed $U = 30.4$ m/s and the radius $R_0 = 4.7$ mm.

Examples of the average wave profiles (thick) over ten data sets observed at six θ positions are shown in figure 15 together with their r.m.s. error curves (thin). Figure 16 shows a comparison between the (averaged) observed curve and the predicted profiles on absolute scales for the same vortex as in figure 14. The observation was made at $x = 634$ mm. The solid curve is the experimental profile $a_*(t)$ and the broken curves are the computed ones $p/F(\theta, \phi = 90°)$ obtained by using (6.5) for the relative core sizes $\delta_0/R_0 = 0.2$ (thin broken) and 0.3 (thick broken). It is found that the theory

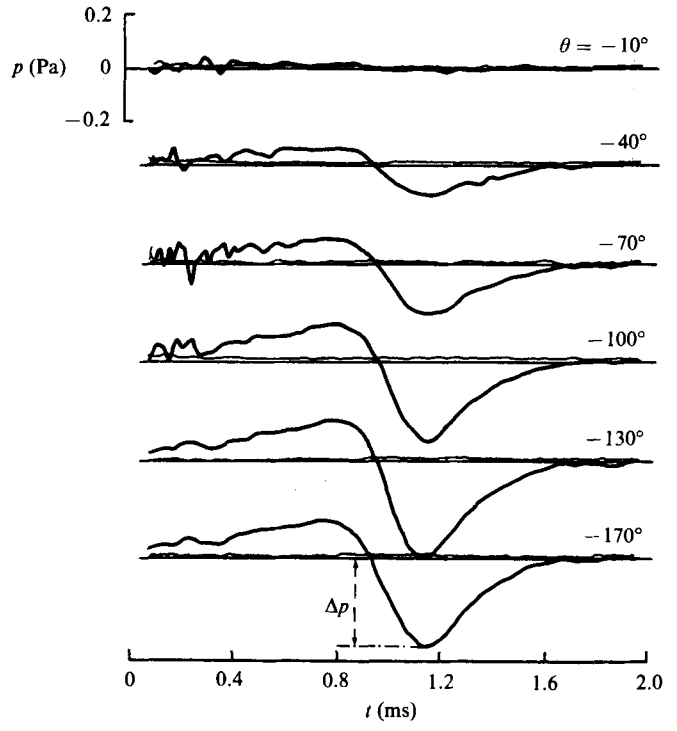

FIGURE 15. Examples of average wave profiles (thick) and their r.m.s. error curves (thin) at six θ positions ($\phi = 90°$) for $U = 30$ m/s, $x = 634$ mm and $L = 9.6$ mm.

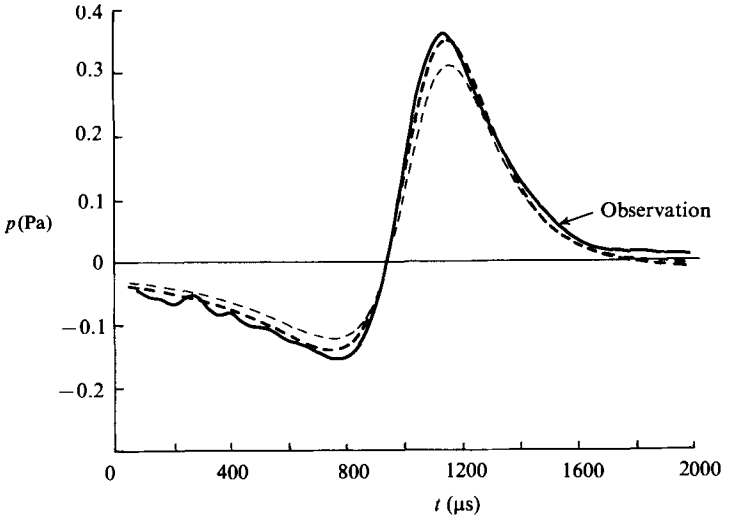

FIGURE 16. Comparison between observed (solid) and predicted (broken) profiles. The solid curve is $a_*(t)$. $U = 30.4$ m/s, $R_0 = 4.7$ mm, $x = 634$ mm, $\delta_0/R_0 = 0.2$ (thin broken) and 0.3 (thick broken).

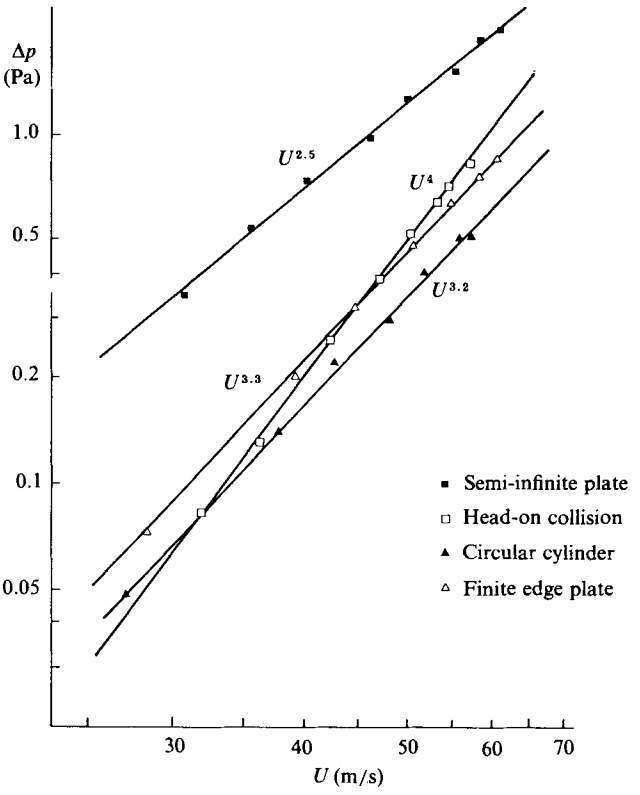

FIGURE 17. Observed laws of the acoustic pressure amplitude Δp versus the translation speed U (in an isolated state). The power laws shown in the diagram correspond to the straight lines.

can predict the main features of the observations. This verifies that the wave profile is determined by the $\frac{3}{2}$th time derivative of the volume flux J through the vortex.

7. Summary

Fundamental aspects of sound emission by vortex motions are considered. Three typical cases of vortex sound are examined in detail: sound emissions by (i) vortices in free space, (ii) vortex–body interaction and (iii) the interaction of vortex with an edged body of semi-infinite extent. The main theoretical predictions including wave profiles and directionalities are reproduced in laboratory experiments.

In particular, we show in figure 17 the experimental power laws of the acoustic pressure amplitude Δp (see figures 3, 10, 15) versus the translation speed U of a single vortex (far from a body). It is found that the curves for head-on collisions and edge–vortex interactions are well described by the power laws (4.11) and (6.8), and that the curve of vortex–cylinder interaction closely follows the predicted power law (5.11). Note that the peak values Δp shown here were obtained at fixed angles (not the average over the angles), and that in the case of the head-on collision the relative speed should be doubled.

The present consideration is restricted to the motion of an inviscid fluid at low Mach numbers. Viscosity effects are discussed in Morfey (1976), Kambe (1984), Obermeier

(1985) and Minota & Kambe (1986). The sound generation by high-speed flows is outside the scope of the present paper.

Our recent studies using simple fluid-dynamical systems presented here include both theoretical and experimental investigations. In view of the aim of the Symposium, the usefulness of such a combined study to obtain concrete results should be especially emphasized. This work is cordially dedicated to the spirit of that great scientist G. I. Taylor. The author is grateful to Miss T. Minota for her invaluable contributions to the experimental and computational aspects of the work.

REFERENCES

CRIGHTON, D. G. 1972 *J. Fluid Mech.* **51**, 357–362.

CRIGHTON, D. G. & LEPPINGTON, F. G. 1970 *J. Fluid Mech.* **43**, 721–736.

CROW, S. C. 1970 *Stud. Appl. Math.* **49**, 21–44.

CURLE, N. 1955 *Proc. R. Soc. Lond.* A **231**, 505–514.

DYSON, F. W. 1893 *Phil. Trans. R. Soc. Lond.* A **184**, 1041–1106.

FFOWCS WILLIAMS, J. E. 1969 *Ann. Rev. Fluid Mech.* **1**, 197–222.

FFOWCS WILLIAMS, J. E. & HALL, L. H. 1970 *J. Fluid Mech.* **40**, 657–670.

HOWE, M. S. 1975*a* *J. Fluid Mech.* **67**, 597–610.

HOWE, M. S. 1975*b* *J. Fluid Mech.* **71**, 625–673.

KAMBE, T. 1984 *J. Sound Vib.* **95**, 351–360.

KAMBE, T. & MINOTA, T. 1981 *J. Sound Vib.* **74**, 61–72.

KAMBE, T. & MINOTA, T. 1983 *Proc. R. Soc. Lond.* A **386**, 277–308.

KAMBE, T., MINOTA, T. & IKUSHIMA, Y. 1985 *J. Fluid Mech.* **155**, 77–103.

KAMBE, T., MINOTA, T. & IKUSHIMA, Y. 1986 In *Proc. IUTAM Symp. on Aero- and Hydro-acoustics, Lyon 1985* (eds. G. Comte-Bellot & J. E. Ffowcs Williams). Springer.

LAUVSTAD, V. R. 1968 *J. Sound Vib.* **7**, 90–105.

LIGHTHILL, M. J. 1952 *Proc. R. Soc. Lond.* A **211**, 564–587.

MACDONALD, H. M. 1915 *Proc. Lond. Math. Soc.* **14**, 410–427.

MINOTA, T. & KAMBE, T. 1986 *J. Sound Vib.* **110**, (in press).

MIYAZAKI, T. & KAMBE, T. 1986 *Phys. Fluids* (in press).

MÖHRING, W. 1978 *J. Fluid Mech.* **85**, 685–691.

MÖHRING, W., MÜLLER, E.-A. & OBERMEIER, F. 1969 *Acustica* **21**, 184–188.

MORFEY, C. L. 1976 *J. Sound Vib.* **48**, 95–111.

MÜLLER, E.-A. & OBERMEIER, F. 1967 *AGARD Conf. Proc.* **22**, 22.1–22.8.

NOBLE, B. 1958 *Methods Based on the Wiener-Hopf Technique.* Pergamon.

OBERMEIER, F. 1967 *Acustica* **18**, 238–240.

OBERMEIER, F. 1976 In *Singular Perturbations and Boundary Layer Theory.* Lecture Notes in Mathematics, vol. 594, pp. 400–421. Springer.

OBERMEIER, F. 1979 *Acustica* **42**, 56–71.

OBERMEIER, F. 1980 *J. Sound Vib.* **72**, 39–49.

OBERMEIER, F. 1985 *J. Sound Vib.* **99**, 111–120.

POWELL, A. 1964 *J. Acoust. Soc. Am.* **36**, 177–195.